Modelling Convection Over Arctic Leads With LES and a Non-Eddy-Resolving Microscale Model

C. Lüpkes,[1] V.M. Gryanik,[1,2] B. Witha,[3] M. Gryschka,[3] S. Raasch,[3] and T. Gollnik[1]

published in:

J. Geophys. Res., 113, C09028, doi:10.1029/2007JC004099

C. Lüpkes, Alfred Wegener Institute for Polar and Marine Research, Postfach 120161, D-27515 Bremerhaven, Germany. (Christof.Luepkes@awi.de)

[1]Alfred Wegener Institute for Polar and Marine Research, Bremerhaven, Germany

[2]A.M. Obukhov Institute of Atmospheric Physics, Russian Academy of Sciences, Moscow, Russia

[3]Institute of Meteorology and Climatology, University of Hannover, Germany

Abstract. Turbulent heat transport over inhomogeneous surfaces with sharp temperature discontinuities is investigated with a focus on the flow over leads in sea ice. The main goal consists in the development of a turbulence closure for a microscale atmospheric model resolving the integrated effect of plumes emanated from leads, but not the individual convective eddies. To this end ten runs are carried out with a Large Eddy Simulation (LES) model simulating the flow over leads for spring time atmospheric conditions with near-neutral inflow and a strong capping inversion. It is found that leads contribute to the stabilizing of the polar atmospheric boundary layer (ABL) and that strong countergradient fluxes of heat exist outside a core region of the plumes. These findings form the basis for the development of the new closure. It uses a new scaling with the internal ABL height and the characteristic vertical velocity for the plume region as the main governing parameters. Results of a microscale model obtained with the new closure agree well with the LES for variable meteorological forcing in case of lead-orthogonal flow and for a fixed ABL height and lead width. The good agreement concerns especially the plume inclination, temperature and heat fluxes as well as the relative contributions of gradient and countergradient transport of heat. A future more general closure should account e.g., for variable lead widths and wind directions. Results of the microscale model could be used to derive a future parameterization of the lead effect in large scale models.

1. Introduction

A large part of the Arctic Ocean is covered permanently with pack ice. But due to divergent sea ice drift, even during winter open water areas exist, which are called leads or polynyas depending on their shape. The length of leads varies between hundreds of meters and hundreds of kilometers, and their width ranges from several meters to kilometers. A typical sea ice situation in springtime is displayed in Figure 1 by an image of the satellite Aqua Modis obtained on 16 April 2005 about 100 km northeast of Svalbard. The three largest leads in this image have a length of approximately 150 km. Leads are either free of ice or at least covered by thin new ice only. Between late autumn and spring the surface temperature of open water and of new thin ice is much larger than the air temperature. Due to the large temperature differences of up to 40 K, strong turbulent convection is generated above the leads, which penetrates into the slightly stable or neutral shallow atmospheric polar boundary layer, and thus, significantly modifies its structure.

Since leads are observed everywhere in the pack ice and at any season, they can have a large influence on the energy exchange between the polar ocean and the atmosphere [*Lüpkes et al.*, 2008]. With respect to climate modelling it seems necessary to gain a detailed understanding of the atmospheric processes in the environment of an ensemble of leads and especially to investigate the transport of heat by convective plumes above and downstream of typical individual leads.

Convection above leads has been studied in the past by observations and modelling. Observations and their analysis concentrated mainly on the near-surface processes over leads [*Paulson and Smith*, 1974; *Andreas et al.*, 1979; *Ruffieux et al.*, 1995; *Alam and*

Curry, 1997; *Persson et al.*, 1997; *Pinto et al.*, 2003]. These studies show that there is a strong influence of leads on the downstream near-surface profiles of wind speed and temperature and that heat fluxes over leads range in the order of hundreds of W m^{-2}. Based on data analyses *Andreas and Murphy* [1986] and later *Andreas and Cash* [1999] proposed a parameterization of the surface layer transfer coefficients of heat as a function of the non-dimensional fetch in the lead. They found that coefficients increase with decreasing fetch. The fetch dependence of the surface heat fluxes was confirmed by *Alam and Curry* [1997], who derived the heat transfer coefficients applying surface renewal theory to the air-sea interface. Drag coefficients were derived as a function of various parameters e.g., the wave age, which is also fetch dependent.

An improved understanding of the impact of leads on the atmospheric boundary layer (ABL) requires a consideration of processes in the entire ABL rather than of the near-surface processes only. This has been done in the past with high resolution 2D models [*Zulauf and Krueger*, 2003] and with large eddy simulation (LES) models, since observations of the flow across leads were not available with sufficient resolution for a detailed data based analysis of processes. *Glendening and Burk* [1992] as well as *Weinbrecht and Raasch* [2001] simulated convective processes with LES above small scale (200 m width) leads for non-zero geostrophic wind, prescribing a stably stratified ABL in the lead environment with a height constant vertical temperature gradient. *Esau* [2007] studied processes over leads of different widths, but for zero geostrophic wind. Conditions in a real arctic environment are often characterized, however, by a slightly stable or close to neutral ABL of 50 m to 500 m thickness, which is capped by a strong inversion. Moreover, in arctic regions strong wind speeds occur much more often than light winds [*Lüpkes et al.*, 2008].

Thus, the first goal of our present investigation is to model convection with LES over leads using observed inflow profiles with a neutral lower layer capped by an inversion at 300 m. We consider conditions with wind speeds strong enough to avoid a recirculation as that modeled by *Esau* [2007]. The lead width will be prescribed to 1 km, which is typical for conditions in the Fram Strait pack ice region [*Lüpkes et al.*, 2004].

The second goal is the development of a turbulence closure for microscale modelling of the flow over leads resolving only the integrated effect of plumes emanated from leads but not the individual convective eddies as in LES. This is done for two reasons. The first is that the microscale modelling helps to gain additional insight into the governing processes related to the flow over leads. This is of fundamental importance for the future derivation of parameterizations of the lead influence to be used in climate models. The second reason is that the application of LES models is restricted to a relatively small domain, whereas a microscale model could be used later to investigate the impact of an ensemble of leads in domains much larger than that possible for LES models.

We use a 2D-microscale model with 200 m horizontal grid spacing to model the convection over leads with 1 km width similar as *Mauritsen et al.* [2005] in their study of internal gravity wave generation by leads. Convective eddies cannot be resolved with such grid sizes, and a priori, it is not clear, to what extend the results of such a model can be realistic. Classical turbulence closures have been developed for horizontally quasi-homogeneous turbulence. However, strong horizontal gradients of wind, temperature, stratification, and turbulent fluxes exist over sea ice with leads. A schematic representation of the typical flow regimes above a lead is given in Figure 2 showing the slightly stable or neutral region upstream of a lead, a tilted plume region with strong convection and an outflow region, which is again slightly stable or neutral. It can be expected that turbulence closures have to be adjusted to the typical atmospheric conditions in such an environment.

We will present at the end a closure accounting for this complex flow structure. It is nonlocal in the plume region and local for its close environment. Still, its applicability will be tested for a few idealized cases only, but it can be considered as a first step towards a more general closure to be used in microscale models for convection over inhomogeneous surfaces with sharp temperature discontinuities. This work does not consider, how the effect of leads could be treated in large scale numerical models. However, results of the microscale model could be used in the future to develop parameterizations for such models. This is outlined in Section 7.

Overall, our work contains the following topics: a case study with LES of the ABL response on convective heating by leads (i), the development of a new scaling for convective turbulence in the environment of leads and a new parameterization of heat transport above and downstream of leads (ii) and its application to a microscale model (iii). The paper is structured as follows. After a short presentation of the used models (Sections 2 and 3), we explain results of the LES model (Section 4), which is applied to model the flow across a lead. Hereafter, in Section 5 the new turbulence closure is derived and results of the microscale model with the new closure are explained in Section 6.

2. Model Description

2.1. The Microscale Model

We use the nonhydrostatic and anelastic atmospheric model METRAS [*Schlünzen*, 1988, 1990] in a 2D-version as applied earlier to cold air outbreaks by *Lüpkes and Schlünzen* [1996] and by *Birnbaum and Lüpkes* [2002] and to on-ice flow regimes by *Vihma et al.*

[2003]. Its 3D-version was applied to arctic regions by *Dierer and Schlünzen* [2005, 2005a] and by *Hebbinghaus et al.* [2006]. The model is originally a mesoscale model with horizontal grid spacing Δx of at least 1 km in convective conditions. However, we apply it here with $\Delta x = 200$ m to resolve the integrated effect of convective plumes on the ABL above leads. Since the typical scale of flow distortion due to leads is in the order of kilometers, this phenomenon belongs to the microscale α, and we call the model in the following a microscale model. It is non-eddy resolving, since populations of convective eddies or individual plumes are not explicitly modelled, and their integral effect has to be treated via the turbulence parameterization. Hence, the model differs strongly from LES models with much smaller horizontal grid sizes, which are able to resolve convective turbulence, i.e. dynamics of individual plumes. The METRAS version applied here is based on the Boussinesq-approximated primitive equations with potential temperature and three wind components as prognostic variables. We consider neither radiation nor condensation processes while prescribing a dry atmosphere for simplicity.

The model equations are solved on a staggered ARAKAWA-C grid with 10 layers below 300 m and the first layer for temperature and horizontal wind at 10 m height. 34 layers follow above this height, and the model top is at 8000 m, which allows the damping of gravity waves towards the model top.

At lateral boundaries, boundary-normal gradients of boundary-parallel wind components and of potential temperature are prescribed to zero. The boundary-normal wind is derived from the prognostic momentum balance equations.

For initialization, the model requires the large scale geostrophic wind as well as quasi-stationary profiles of potential temperature at the inflow boundaries. Such profiles are determined with the 1D model version based on observed or prescribed meteorological variables and profiles.

We neglect horizontal turbulent transport, since it was found from LES results that in the relevant regions, influenced by convective plumes from leads, vertical turbulent transports are much larger than the horizontal ones. Surface fluxes of heat and momentum are calculated via Monin-Obukhov theory with similarity functions according to *Dyer* [1974]. METRAS can be run with different closures for the calculation of turbulent fluxes above the surface layer. However, the present application of the model requires a new closure adjusted to the special conditions of a nonhomogeneous flow regime over leads. The new closure will be derived in Section 5.

2.2. The LES Model

Besides METRAS, we use the **PA**rallelized **L**arge-eddy simulation **M**odel **PALM** [*Raasch and Schröter*, 2001]. So far, PALM has been applied to study homogeneously [*Schröter et al.*, 2000; *Gryanik et al.*, 2005] and heterogeneously heated convective boundary layers (e.g., *Raasch and Harbusch* [2001]; *Letzel and Raasch* [2003]) as well as the stably stratified boundary layer [*Beare et al.*, 2006]. A former non-parallelized version has already been used by *Weinbrecht and Raasch* [2001] to study the flow above leads. The model equations, the staggered grid, and the boundary conditions including stability functions and roughness length are generally the same as in METRAS (see also next subsection). The subgrid-scale turbulence closure scheme is based on *Deardorff* [1980], using an additional prognostic equation for the SGS turbulent kinetic energy.

The domain size is 40960 m $\times$ 640 m $\times$ 1472 m along x (lead orthogonal), y, and z. The grid spacing is equidistant with 10 m along all directions except the vertical, where it is smoothly stretched above 350 m. The first layer for temperature and the horizontal wind components is at 5 m. Some cases were run also with increased resolution to test the reliability of the coarse resolution runs.

As *Weinbrecht and Raasch* [2001] already showed, a high spatial resolution is required to adequately resolve turbulent elements above the lead. For a lead width of 200 m and their smallest grid spacing of 2 m, they failed to resolve the turbulence even for a comparably small background wind of 5 m s^{-1}. As a compromise between resolution and CPU time requirements, the ratio between lead width (1000 m) and grid spacing (10 m) in the present study is just the same as in the Weinbrecht and Raasch study. Although our simulations are therefore unable to resolve the very shallow convection above the first half of the lead, the grid spacing should nevertheless be sufficient because *Weinbrecht and Raasch* [2001] also found that the qualitative and quantitative structure of the downstream plume does not significantly change for a smaller grid spacing.

The 1D temperature and wind profiles from METRAS are used for initialization. A quasi-stationary state is reached after about 1800 s.

3. Scenarios and Setup of Models

In the present investigation we consider the flow across two leads of 1 km width and 10 km distance to each other. Such leads were often observed by *Lüpkes et al.* [2004] in the Fram Strait region about 100 - 200 km north from the ice edge.

Ten cases were modelled, which differ in the geostrophic wind speed, near-surface ABL temperature at the inflow boundary, and in the surface fluxes of sensible heat over the leads. In all cases, which are summarized in Tables 1 and 2, the flow is approximately orthogonal to the lead in the lowest 100 m. We distinguish between two sets of cases with respect to the thermal situation. In the first one (cold cases) the surface temperature and ABL temperature at the inflow position is prescribed to 250 K over pack ice. In the second set (warm cases) the surface temperature of ice and ABL temperature amount to 260 K. The surface temperature of the lead is always assumed as 270 K, which is lower than the freezing point, since often a layer of very thin ice or grease ice is developing above newly formed leads.

In all cases, we assume a neutral boundary layer at the inflow boundary of the first lead, which is capped by a strong inversion at 300 m height. Such a profile was observed by aircraft during the campaign ARTIST [*Hartmann et al.*, 1999, *Wacker et al.*, 2005] over the northern Fram Strait pack ice region. For simplicity and since our present focus is on the investigation of the heat transport in higher levels, we decided to neglect the fetch dependence of roughness (see introduction) and prescribe in both models the roughness lengths for momentum to $z_0 = 10^{-3}$ m over pack ice and $z_0 = 10^{-4}$ m over the lead. The roughness length for heat is assumed as one tenth of z_0, which is also a simplification of reality (see e.g., *Andreas and Murphy* [1986] and *Andreas and Cash* [1999]).

In both models the same lateral boundary conditions (zero gradient) and initial profiles are used. However, the LES slightly modifies these profiles in the inflow region, since it produces its own stationary solution and turbulence is too weak in the inflow region (boundary about 10 km in front of the first lead) to be resolved by the LES. To trigger the turbulence development the vertical velocity is disturbed randomly in the first kilometer of the domain as in *Weinbrecht and Raasch* [2001]. Moreover, at the upstream side of the second lead large eddies, generated over the first lead, naturally produce in our simulations a well mixed ABL with turbulence being resolved by the LES. In other words, the first lead plays the role of a natural trigger mechaninsm in our simulations, which is stronger than the triggering by white noise. When we compare results of METRAS and of the LES we concentrate, therefore, on the region over the second lead. We found that the impact of differences between the inflow profiles of METRAS and of the LES at the upstream side of the second lead on fluxes and temperatures are small compared with the lead impact. For example, the maximum difference in temperatures is only 0.2 K, which can modify the surface fluxes in the considered parameter range by 1-2 % only.

For simplicity, the models are run in their dry version with zero humidity. This is a further simplification, but not too restrictive. During the cruise ARKTIS XIX/1 with RV Polarstern in spring 2003 convection was observed very often over leads in the Barents Sea and Fram Strait pack ice without the formation of clouds or sea smoke [*Lüpkes et al.*, 2004].

4. Results of the LES Model

In Figures 3 - 5 only those averaged fields of variables obtained with the LES are presented, which will later be compared with results of the microscale model. The averaging period is 900 s as in *Weinbrecht and Raasch* [2001]. Spatial averaging is done parallel to the lead (orthogonal to the incoming wind) across the entire domain.

Figures 3 and 4 show the potential temperature, the vertical turbulent fluxes of sensible heat (sum of subgrid scale and resolved contribution) and the horizontal wind speed for the weak-wind, medium-wind and strong-wind cases of the cold data sets (Table 1). In all figures the inflow is directed from left to right and the lead position is from 0 to 1 km distance. The topological structure of the quasi-stationary solutions seems to be similar in all cases. There is a strong plume with upward fluxes in the order of 100 W m^{-2} in its core

(Figure 3). Obviously, the plumes penetrate slightly into the inversion while generating turbulence and consequently an entrainment flux, which is visible in the figures by negative (downward) fluxes on top of the plumes. One can distinguish well pronounced boundaries of the plume separating the convection dominated regions from the environment. In the weak-wind case the plume shape is more symmetric with respect to its centerline than in the strong-wind case, where the turbulence is advected over a larger region downstream of the lead than in the weak-wind case. Differences between the three cases are related mainly to the inclination of the plume centerline and magnitude of surface heat fluxes. The plume inclination increases with increasing wind and decreases with increasing surface heat flux. The sensitivity to a variation of the wind speed is larger than to a variation of the surface heat flux (see Table 1).

Within the most part of the modelled ABL the potential temperature increases slightly with height. An unstable stratification (Figures 3 and 5) is found only in the plumes' core.

Figures 3 and 5 illustrate that the vertical component of heat fluxes in the plume are directed partly along the vertical temperature gradient (downgradient) and partly countergradient. The occurrence of countergradient fluxes is independent on the wind. In the strong-wind case the region of countergradient fluxes occurs more on the downstream end of the plume, whereas in the weak-wind case a more symmetric distribution of downgradient and countergradient regions is found. In all cases the horizontal component of heat fluxes (not shown) are small in and outside of the convective plume region.

Also the fields of horizontal wind have a similar topological structure in all cases (Figure 4). In the lowest 80 m the lead causes horizontal gradients in wind speed. However, wind speeds vary only slightly in the layer between 80 m and 250 m. In all cases the vertical velocity (not shown) turned out to be small (in the order of millimeters to centimeters per second). This is due to the averaging in lead parallel direction, which cancels out the effect of updrafts and downdrafts in the convective eddies.

The general flow features including the occurrence of countergradient fluxes are qualitatively similar to the results shown by *Glendening and Burk* [1992] and by *Weinbrecht and Raasch* [2001]. Quantitative differences can be attributed to the smaller lead width in the latter studies and to differences in the meteorological conditions such as the prescribed initial stratification.

5. Turbulence Closure for Microscale Modelling of Convection over Leads

5.1. Studies with Existing Closures

The LES results (Figure 5) clearly show the occurrence of countergradient heat fluxes. It is well known (e.g., *Holtslag and Moeng* [1999], *Zilitinkevich et al.* [1999], *Van Dop and Verver* [2001]) that such fluxes, which are independent on the local gradients of temperature, can only be parameterized with a nonlocal closure. Nevertheless, we used the microscale model in a first step with different local closures to clearly identify the drawbacks. We applied a simple first order mixing length closure, summarized in Appendix A, and closures based on the prediction of turbulent kinetic energy such as the 1.5th order closure (level 2.5) of *Mellor and Yamada* [1974] and the closure of *Teixeira and Cheinet* [2004]. The results of such model runs were all similar. There was a fair representation of the wind field similar as that shown in Figure 7, but a temperature increase with height as in the LES could never been obtained. Furthermore, the heat fluxes were either underestimated or - after tuning the maximum mixing length - the plume inclination became too weak. It became obvious that an improvement of closures should account for the nature of nonlocal countergradient heat transport within the plumes.

The most simple closures allowing countergradient heat transport are those, which are based on the heat transport equation

$$\overline{w'\Theta'} = -K_H \left(\frac{\partial \overline{\Theta}}{\partial z} - \Gamma \right) . \tag{1}$$

$\overline{w'\Theta'}$ is the turbulent heat flux and K_H is the eddy diffusivity for heat. Γ is sometimes called countergradient term, but this is misleading, since $K_H\Gamma$ is always an upward heat flux independent on the sign of the temperature gradient. Hence, we refer to $K_H\Gamma$ in the following as the nonlocal or nongradient flux and to $K_H(d\Theta/dz)$ as the local or gradient flux.

There are several closures in literature using the above formulation. They differ mainly by the formulation of K_H and Γ. We tested the schemes of *Troen and Mahrt* [1986] and *Lüpkes and Schlünzen* [1996], henceforth abbreviated by LS96. The latter is used as a basis for a an improved closure for lead convection and is therefore described here in detail.

Equations for K_H and Γ of LS96 can be written in nondimensional form as a function of the stability parameter $S = w_*/u_*$, where u_* is the friction velocity and w_* the convective velocity scale [*Deardorff*, 1970] given by

$$w_* = (\frac{g}{\Theta_0} z_i \overline{w'\Theta'}|_s)^{1/3} = (B_s\, z_i)^{1/3} . \tag{2}$$

$B_s = (g/\Theta_0)\overline{w'\Theta'}|_s$ is the surface buoyancy flux, z_i is the mixed layer depth. We obtain (see Appendix B)

$$K_H/K_p = Z\,(1 + \frac{S}{\kappa} Z^{1/3})\,(1 - Z)^2 \quad, Z_p \leq Z \leq 1 \tag{3}$$

with the nondimensional vertical coordinate $Z = z/z_i$ and the eddy diffusivity at the surface layer top z_p

$$K_p = u_* \kappa z_p / \Phi_p \tag{4}$$

with $\Phi_p = (\Phi_H|_{z_p} + \Phi_\Gamma)\, Z_p\, (1 + (S/\kappa) Z_p^{1/3})\, (1 - Z_p)^2$. Φ_H is the Monin Obukhov similarity function for heat and $\Phi_\Gamma = \Gamma|_{z_p}\, \kappa\, z_p\, u_*\, /\, \overline{w'\Theta'}|_s$. Due to the above K_H-formulation, a matching of heat fluxes with surface layer fluxes is achieved, which guarantees continuity of fluxes with height at z_p.

The nonlocal term Γ is parameterized as

$$\Gamma/\Gamma_0 = 0.63\, b\, S \Big[(1 - Z)^{3/2} + 0.593\, S^3 Z\, (1 - 0.9Z)^{3/2} \Big]^{-2/3} , \tag{5}$$

where $\Gamma_0 = (\overline{w'\Theta'}|s)/(u_* z_i)$. In equations (3), (4), and (5) the stability parameter S represents the relative importance of convective and mechanical mixing.

It is important to note that with equations (3) - (5) the forcing of turbulence is related at any position with coordinates (y, z) to the properties of the surface at location $(y, 0)$, where y and z are the horizontal and vertical coordinates, respectively. Thus, application of the nonmodified LS96 scheme to the microscale model simulating the flow over leads restricts the plume region to the lead region and generates a non-inclined plume, since downstream of the lead the surface heat flux is close to zero or even negative. This is in large contrast to the LES results showing an inclined plume.

5.2. A new closure

5.2.1. Principles

Motivated by the above results with existing closures a new closure was developed, which is based on the following principles:

1. Heat transport in convective plumes originating from a lead (grey shaded in Figure 2) is dominated by nonlocal effects, while farer away from the plumes mixing is local. As the basic scheme in the convective core region, we use the closure by LS96, which is adopted to the nonhomogeneous conditions. At the boundaries of the plume, we switch to a local closure (in this paper to that described in Appendix A).

2. The switching lines are given by the local heights of the internal boundary layers $\delta(y)$ (upper plume boundary) and $\delta_d(y)$ (lower plume boundary) with $y =$ distance from the lead's upstream edge.

3. The functional forms of the vertical profiles of the eddy diffusivity for heat K_H and of the nonlocal term Γ at each position above and downstream of the lead remain the same as over a homogeneous surface, but K_H and Γ are scaled with the fetch dependent $\delta(y)$ instead of z_i. The fetch dependence of K_H and Γ is accounted for by introducing a fetch dependence of the stability parameter $S = S(y)$.

4. Dominating parameters for the processes in the convective core region above and downstream of the lead are: the surface buoyancy flux over the lead $B_l = g/\Theta_0\, \overline{w'\Theta'}|_l$, the vertically integrated mean horizontal velocity at the lead's upstream edge U, and the inversion layer height z_i.

5. We consider in the present paper only cases with neutral stratification in a shallow ABL capped by an inversion strong enough to avoid convection from penetrating a long distance into the inversion layer. Hence, stratification within the shallow ABL does not appear as parameter, and we prescribe z_i as constant.

6. Momentum fluxes are determined with a local closure (Appendix A), which is applied to the entire domain.

5.2.2. Internal Boundary Layer Heights and Stability Parameter

To realize the above principles for the nonlocal closure and its matching with the local one, the stability parameter S and the internal boundary layer height δ should be specified as functions of y. The largest difficulty in defining S and δ consists in the correct introduction of the characteristic vertical velocity scale, which occurs in both S and δ.

Our approach is as follows. For $0 < y < L$, the velocity of the convective eddies may be taken as equal to the same velocity as used in homogeneous conditions, namely $w_l = (B_l\delta)^{1/3}$, where we use subscript l instead of asterisk $*$ to avoid confusion with the Deardorff scale w_* (Equation 2). This scale is reasonable, because the largest eddies have a horizontal scale smaller than 2δ and $2\delta < L$, thus the assumption of homogeneity can be used in that region. However, for $y > L$, due to lateral entrainment and dissipation, the characteristic convective velocity is reduced in comparison with w_l in the region $0 < y < L$. We express this reduction by an exponential decay function and take the characteristic convective velocity scale as

$$w_l(y) = c\,(B_l\,\delta)^{1/3}\ \exp(-(y/D))\ , \tag{6}$$

where D is the decay length scale to be specified below. c is an adjustable constant. We can use equation (6) in the full range $y > 0$ for small leads.

δ and the decay length scale D are derived as follows. We assume that the local inclination angle of the plume boundary $\phi \approx tg(\phi) \approx d\delta/dy$ is equal to $w_e/(U + u_e)$, where U is the mean horizontal velocity at the upper plume boundary and w_e and u_e are the entrainment vertical and horizontal velocity at the same boundary. Furthermore, in the range of parameters studied $u_e \ll U$ in accordance with LES data (not shown). Thus, the internal boundary layer equation (see also *Monin and Yaglom* [1971]; *Turner* [1986]) reads

$$\frac{d\delta}{dy} = \frac{w_e(y)}{U} \, . \tag{7}$$

Furthermore, we assume that δ is influenced by the strongest convective eddies in the plume, whose vertical velocity is w_{max}. Thus, we can write $w_e = a_e \, w_{max}$, where a_e is constant. Finally, we use the assumption that w_{max} is scaled with the characteristic convective velocity (6) as $w_{max} = a_m \, w_l$, where a_m is also an adjustable constant. After expressing now w_e in terms of w_l, using (6) in (7), and integration with the boundary condition $\delta = 0$ for $y = 0$, we obtain

$$\delta(y) = \delta_{max} \, (1 - \exp(-y/D))^{3/2} \tag{8}$$

with the plume penetration height

$$\delta_{max} = \Big(\frac{2a}{3} \, \frac{B^{1/3} D}{U}\Big)^{3/2} \, , \tag{9}$$

where $a = a_e\, c\, a_m$. Since in a neutral environment convective turbulence always penetrates up to the inversion, we can set $\delta_{max} = z_i$ in equation (9). We find then the decay length scale as

$$D = \frac{3}{2a}\left(\frac{U^3}{B_l}\right)^{1/3} z_i^{2/3} \ . \tag{10}$$

The length scale D has a simple physical meaning: $D \approx U\tau$, where $\tau \approx z_i/w_* \approx z_i^{2/3}/B_l^{1/3}$ is the eddy turnover time of the largest available convective eddies in the plume. Finally, with the constraint of maximal penetration $\delta_{max} = z_i$, equation (8) reads

$$\delta(y) = z_i\,(1 - \exp(-y/D))^{3/2} \tag{11}$$

with D given by equation (10). Due to equation (11) $\delta(y)$ is independent from z_i, if $y \ll D$, namely $\delta(y) \approx z_i(y/D)^{3/2} = (2a/3)^{3/2}(B_l^{1/2}/U^{3/2})y^{3/2}$. Furthermore, $\delta(y) \approx z_i$, if $y \gg D$.

As mentioned above, we match the nonlocal closure with the local closure downstream of the plume. We introduce the downstream lower boundary of the plume $\delta_d(y)$ by the constraint

$$\overline{w'\Theta'}_{ng}|_{z=\delta_d} = K_H\,\Gamma|_{z=\delta_d} = \overline{w'\Theta'}_{crit} \ , \tag{12}$$

where $\rho c_p \overline{w'\Theta'}_{crit} = F_{crit}$ is some threshold value close to zero. This definition of the plume boundary is based on the analysis of LES data showing that heat fluxes are predominantly non gradient fluxes at the lower plume boundary δ_d (Figure 5).

It is possible to give an a priori estimation of the constants a and c. First, constant c can be estimated as $c \approx 1.6 \pm 0.5$ (see Appendix C). This is based on the assumption that in the core of the plume convective turbulence is fully developed and similar to convective turbulence over homogeneous surfaces. The constant a_e characterizes the entrainment and is in the range 0.2-0.4 (see *Turner*, 1986). The constant a_m depends on the shape of the vertical velocity profile in the plume, and it is between 2 and 4 for reasonable profiles. Thus, $a = a_e\, c\, a_m$ is defined by three different processes and is in the range between 0.4 and 3.4. It can be expected that the critical heat flux F_{crit} is a few percent only of the surface flux over the lead.

5.2.3. Parameterization in the Convective Region

To arrive at the equations of the new parameterizations, one has simply to replace z_i in the equations of the LS96 closure (section 5.1) by $\delta(y)$. The surface heat flux and the friction velocity occurring in these equations represent now average values above the lead surface. The new scheme consists then of equations (1) and (3) - (6), with $Z = z/\delta(y)$ and with $S = w_l(y)/u_{*,l}$, where index l refers to the lead surface. $\delta(y)$ is given by equation (11) and $\delta_d(y)$ is defined by equation (12). Practically, equation (12) does not have to be solved for δ_d, but when the non-gradient heat flux is lower than F_{crit} the local closure has to be used.

The closure in the convective region depends on three constants, b in equation (5), c in equation (6), and a in equation (10). The possible range of values for these constants has been estimated above. To confirm and optimize these values, at first the weak-wind, medium-wind, and strong-wind cases of the cold situation were modelled (Table 1). The constants were determined as $a = 2.3$, $b = 0.6$, $c = 1.6$. Note that the value for c is equivalent to its value estimated before in Section 5.2.2. Hereafter, it was shown that the optimum values for these reference cases are still valid in the remaining seven cases covering the parameter range, for which the parameterization has been derived. F_{crit} was determined as 2 W m^{-2} for all cases.

5.2.4. Matching With the Surface Layer and With the Local Closure

In the region outside of the plume the local closure is used as described in Appendix A. The plume boundaries are defined by δ and δ_d. At the upper boundary the eddy diffusivities for heat, and hence, the heat fluxes go to zero. The latter behaviour is approximately achieved also at the lower boundary by use of the decay function. Since we consider convection in a neutral or slightly stable environment, heat fluxes are also small or zero outside the plume, where the local closure is applied. Thus, an implicit matching is obtained.

At the lead surface ($0 < y < L$) the heat fluxes match with the surface fluxes obtained from Monin Obukhov theory, since this property of the parameterization is already prescribed in the LS96 closure.

6. Results of the Microscale Model Obtained With the New Closure

6.1. Cold Cases

In Figures 6 and 7 results of the three reference runs (weak-wind, medium-wind, strong-wind) are presented, which were obtained with the closure as described in the previous section using equations (1) and (3) - (6) and with constants a, b, c, set to the optimum values 2.3, 0.6, and 1.6 as mentioned above. According to the figures, the overall structures of the modelled fields agree well with those of the LES solution. As in the LES results the potential temperature increases with height downstream of the lead and an unstable stratification occurs only in a small region in the plume's core. The inclination of the plumes marked by upward heat fluxes agrees well with the LES results in all cases. The inclination angle decreases with increasing wind speed as in the LES. Also the amount of fluxes is well reproduced (Table 1). In the reference runs, the deviation of the maximum fluxes at 200 m and 100 m between both models is in the order of 10 % with a general underestimation of fluxes at 100 m. However, this points more to a slight problem with the LES rather than to a failure of the parameterization. Close to the surface, the LES cannot resolve convection within the first 100 m distance over the lead. This results in an unrealistic peak in the fluxes further downstream, which is still slightly visible at 100 m height. A further investigation with increased LES resolution showed indeed a weakening of near-surface heat flux maxima.

In Figure 5, the regions with fluxes along the gradient and counter to the gradient are shown, which result from the microscale model with the new closure. These regions agree fairly well with the corresponding LES results shown in the same figure.

Two further cold cases were considered. In case 2 (Table 1) the quality of agreement between the microscale model and LES results is similar as in the reference cases. Only in case 5, which is the case with the strongest wind, fluxes are strongly overestimated by METRAS at 200 m height. However, as already described by Weinbrecht an Raasch (2001), this might also be a sign that the LES resolution for the strongest wind should be better than the used one.

6.2. Warm Cases

In Figures 8 and 9 results are presented for the same forcing wind speeds as in the cold cases, but now for significantly warmer conditions (see also Table 2). Heat fluxes over the lead amount now to less than 50 % of the values in the cold cases. The plume inclination angles decrease in comparison with the cold cases. This result can be expected, since the characteristic convective velocity w_l decreases with decreasing heat fluxes over the lead. The quality of agreement remains approximately the same as in the cold cases. This concerns the absolute values of fluxes, the inclination of the plumes, and the topology of the temperature distribution. But in the weak-wind case the increase of temperature with height is slightly overestimated by the microscale model. It should be emphasized that the same set of constants has been used as in the cold cases. The sensitivity on different values of these constants is described in the following for some of the cold cases.

6.3. Sensitivity Studies

To test the sensitivity on the nonlocal fluxes, we used the new closure with different values of the proportionality constant b in equation (5). According to the results for the medium-wind case, shown in Figure 10, b can be increased by 50 % without a change of the qualitative structure of results, but an increase of b causes a stronger increase of temperature with height. This is due to the redistribution of heat in the ABL from lower levels to higher levels. Hence, an increase of b results in lower temperatures close to the surface and in higher values in the upper third of the ABL.

The sensitivity of the model results was also tested on the inclination of the plume by a variation of parameter a (equation 7). Furthermore, different values were used for c, the parameter occurring in the decay function (6). Typical results are shown in Figures 11 and 12. A strong variation of c by about ± 25 % modifies the fluxes only slightly. The stability downstream of the lead increases with increasing c. A modification of a by ± 15 % has a moderate effect on both fluxes and temperature. Fluxes at 100 m height increase by about 10 %, when a is altered from 2.0 to 2.6 (medium-wind case).

We found, furthermore, that there is only a weak sensitivity of the results to the threshold value of the nongradient heat flux F_{crit} (equation (12)) introduced to separate the plume region from the outer region. An effect of a modified value was visible in the wind fields, where the modelled peak above the lead was less pronounced, when we increased the plume region considerably by reducing F_{crit} from its value 2 W m^{-2} used for the runs shown in the figures to a value close to zero.

Obviously, the structure of model results is very robust against changes of constants. The largest sensitivity is on b, whereas the sensitivity to variations of a, c and of F_{crit} is small.

We tested also the sensitivity of the results on different formulations of the nonlocal term Γ. E.g., we used the *Troen and Mahrt* [1986] formulation of Γ, first together with the present eddy diffusivity (Equation 3). We obtained the same qualitative structure of results, but it was not possible to get the same good agreement with the LES results in all wind cases using only one set of constants. An optimal choice of constants for the strong-wind case led to a strong overestimation of the stratification for the weak-wind case. Finally, we tried to apply the complete scheme of *Troen and Mahrt* [1986] including their eddy diffusivity with appropriate modifications as in section 5.2 for the LS96 scheme. This did not work, however, and this failure could be traced back to the too low values for the eddy diffusivity of heat, which resulted from such a modified Troen and Mahrt closure. This is in contrast to an application of the scheme in homogeneous convective conditions. LS96 showed that in such conditions the lower eddy diffusivities, and hence, the lower local fluxes in the Troen and Mahrt scheme could be compensated by a larger nonlocal flux.

6.4. Nonlocal Momentum Transport

The LS96 closure for convection above homogeneous regions and that of *Troen and Mahrt* [1986] contain a nonlocal parameterization of the eddy diffusivity for momentum. In the schemes of *Frech and Mahrt* [1995] and of *Noh et al* [2003] countergradient fluxes of momentum fluxes are considered. We tested the new closure also with a parameterization of the nonlocal momentum transport similar as in the LS96 closure (results not shown). However, our results of the present scheme indicate that the wind fields agreed slightly better with LES results, when the nonlocal closure for heat transport was combined with the local closure of Appendix A for the parameterization of momentum fluxes.

6.5. Remarks on the Region of Applicability

We developed and tested the closure up to now only for a limited range of parameters, for which LES runs were available. Hence, the application of the closure including the specification of constants c, b, and a is restricted to the tested range ($L = 1$ km, $z_i = 300$ m, $3\ \mathrm{ms}^{-1} < U < 10\ \mathrm{ms}^{-1}$, $51\ \mathrm{Wm}^{-2} < F_s < 270\ \mathrm{Wm}^{-2}$). In this range the present parameterization does not use the width of the lead L as an external parameter. A future development of the scheme should account for variable lead widths, which would result probably in a specification of the constants in terms of the nondimensional parameters L/z_i and L/D. But this needs a thorough analysis of appropriate LES results for larger leads and smaller ABL heights.

The assumption of small inclination angles for the plume's centerline, used in equation (8) is also crucial for our parameterization. This assumption means that $w_e \ll (U + u_e)$, which is valid for nonzero wind with $U \gg u_e$. In the opposite limiting case of zero or very low winds the investigation of *Esau* [2007] indicates that $u_e \approx w_e$, which means that horizontal entrainment is as important as vertical entrainment. In our case, horizontal advection dominates the horizontal entrainment.

The validity of the closure is also restricted to cases without recirculation effects of the flow as obtained by *Mauritsen et al.* [2005] and which can develop in case of very weak wind and strong fluxes. Furthermore, we consider only cases without an interaction of plumes from different leads. This means that D should be smaller than the distance between leads.

7. Summary and Conclusions

In this paper we studied the effect of leads on the arctic ABL. To this end we carried out LES, developed a new scaling and parameterization based on this, and finally implemented it to a meso/microscale model. Our studies had two main goals. The first was to model an idealized scenario of the flow above leads in the arctic pack ice with an LES model for winter or springtime meteorological conditions. These are characterized in the Fram Strait region often by a close to neutral ABL over pack ice with a strong capping inversion and by large temperature differences between the near-surface air and the lead surface. The second goal was to model the same situation with a microscale model being able to resolve the integrated effect of the developing plumes above leads rather than the individual plumes. This is a non-trivial task, since classical turbulence closures are not developed for regions with strong discontinuous thermal surface inhomogeneities and sharp transition zones from convectively to mechanically dominated flow regimes. Hence, it became necessary to develop a new closure for microscale modelling of the flow over leads.

The LES runs led to the result that the strong convective non-gradient heat transport from leads has a stabilizing effect on the ABL downstream of leads. This increase of potential temperature can only be obtained with a non eddy resolving model by using a nonlocal closure for heat transport. Furthermore, such a closure should account for the internal boundary layers developing downstream of leads. Eddy diffusivities and nongradient fluxes should depend on the distance y to the lead. We developed a new scaling by introducing the y-dependent internal boundary layer height and characteristic vertical velocity for the plume region and used it for the development of a new closure, which is based on the nonlocal closure of LS96 in the plume regions. Outside this region a local closure was applied. With this new unified local plus nonlocal closure it was possible to simulate the mean wind field, temperatures, and heat fluxes in the close environment of leads.

The new closure contains three open constants. We adjusted them using three model runs from the LES. It turned out that one of the constants agreed well with its value estimated from theory. We found then that the same set of constants was working for other cases with different wind and temperature conditions as well. The topology of wind, temperature and fluxes characterized e.g., by the plume inclination and regions with increase and decrease of potential temperature with height could be well reproduced. Also the absolute values of fluxes were not too far from the LES. The generally good agreement of modelled fluxes and temperatures obtained with the new closure can be explained by the correct parameterization of relative contributions of gradient and countergradient transport due to small scale and large scale convective eddies, respectively.

Sensitivity studies showed that the new parameterization is rather robust against modifications of the constants, since at least the overall structure of the modelled fields remained unchanged, when the constants were changed moderately.

Despite the good agreement between the results of the microscale and the LES model, we would like to stress that the present scheme is limited to a restricted range of parameters. Up to now, we considered ten cases, differing considerably by the wind, temperature and by the surface fluxes. But the sensitivity on wind direction, on a variation of z_i, on the stability in the background ABL, and on the lead width was not investigated. We expect that especially in case of larger lead widths, low wind speeds, and stable inflow conditions modifications of the scheme will become necessary in the future. Probably, the constants of the parameterizations have to be specified then in terms of the nondimensional parameters L/z_i and L/D (see Section 6.5). In the present study we concentrated on the impact of single leads. In the future, the microscale model could be applied at low computational costs to a domain being representative for one grid cell of a large scale model to study the integral effect of a series of leads on ABL processes dependent on the external forcing. Thus, the present study represents an important first step towards the future derivation of a more general parameterization of the lead impact on ABL processes, which could be used then in climate and weather prediction models.

Appendix A, Local Mixing Length Closure

The present local closure is described by *Herbert and Kramm* [1985] as well as *Kramm* [1995] with the eddy diffusivities for heat K_H and momentum K_M depending on the stability corrected mixing length l_n

$$K_M = \begin{cases} l_n^2 \, |\frac{\partial v}{\partial z}| \, (1-5Ri)^2 & ,0 \le Ri \le Ri_c \\ l_n^2 \, |\frac{\partial v}{\partial z}| \, (1-16Ri)^{1/2} & ,Ri \le 0 \end{cases} \tag{A1}$$

and

$$K_H = \begin{cases} K_M & , 0 \leq Ri \leq Ri_c \\ K_M\,(1 - 16Ri)^{1/4} & , Ri \leq 0 \ , \end{cases} \tag{A2}$$

where $Ri_c = 0.2$ is the critical Richardson number and l_n the mixing length for neutral stratification. The latter is specified according to *Blackadar* [1962] as

$$l_n = \frac{\kappa z}{1 + \frac{\kappa z}{l_{max}}} \ . \tag{A3}$$

$\kappa = 0.4$ is the v. Karman constant. Based on studies of *Brown* [1996] we parameterize l_{max} as 15 % of the ABL height z_i. *Vihma et al.* [2003] have shown that this closure produced fluxes very close to observed values in the case of on-ice flow with a shallow neutral and stable ABL above sea ice. A comparable quality of results was obtained by *Vihma et al.* [2005] with a similar closure in case of weak convection above sea ice due to cold air advection.

Different from many other local closures, which depend also on the Richardson number, the above formulation of eddy diffusivities guarantees matching of fluxes at the top of the surface layer (first grid level) with surface layer theory, when similarity functions of *Dyer* [1974] are used in the surface layer. In the original formulation equations (A1) and (A2) are restricted to $Ri > -5$, in case of smaller Richardson numbers, originally a free convection parameterization is proposed. We applied the above formulation, however, also for $Ri < -5$ to circumvent unsolved problems of matching the closures for different regimes of Ri.

Appendix B, Reformulation of the LS96 Closure

The LS96 closure uses the heat transport equation (1) with the eddy diffusivity

$$K_H = \frac{\kappa\, u_*\, z_p}{(\Phi_H - \kappa z_p/\Theta_* \Gamma|_{z_p})} \left(\frac{z_i - z}{z_i - z_p}\right)^2 \frac{u_* \kappa z + w_* z_i (z/z_i)^{4/3}}{u_* \kappa z_p + w_* z_i (z_p/z_i)^{4/3}} \,, \quad (z_i \geq z \geq z_p) \,, \tag{B1}$$

where u_* is the friction velocity and Θ_* the characteristic surface layer temperature scale. This formulation was derived on the basis of a K_H-parameterization by *Holtslag and Moeng* [1991]. In contrast to their formulation, it accounts for both mechanical and convective mixing by the terms proportional to u_* and to w_*, respectively, and guarantees matching of heat fluxes between the main part of the ABL and the surface layer fluxes obtained from Monin Obukhov theory.

In LS96, the nonlocal term Γ is parameterized following *Holtslag and Moeng* [1991] as

$$\Gamma = b \frac{w_*}{\overline{\overline{w'^2}}} \frac{\overline{w'\Theta'}|_s}{z_i} \,, \tag{B2}$$

where b is a proportionality constant. b was set to 2 by *Holtslag and Moeng* [1991], but LS96 obtained a better agreement with observations using $b = 3$. The variance of the vertical velocity $\overline{w'^2}$ is approximated in equation (B2) by

$$(\overline{w'^2})^{3/2} = 1.6^{3/2}\, u_*^3 (1 - \frac{z}{z_i})^{3/2} + 1.2\, w_*^3 (\frac{z}{z_i})(1 - 0.9\frac{z}{z_i})^{3/2} \,. \tag{B3}$$

Using nondimensionalization with $z = z_i\, Z$, and introducing the nondimensional stability parameter $S = w_*/u_*$ in the above equations leads to

$$\overline{w'^2} = 1.6\, u_*^2\, [(1 - Z)^{3/2} + \frac{1.2}{1.6^{3/2}}\, S^3\, Z(1 - 0.9Z)^{3/2}]^{2/3} \tag{B4}$$

After substituting equation (B4) in equation (B2), and using again the nondimensionalization, it is straightforward to obtain equations (3) - (5). The constants 1/1.6 and $1.2/1.6^{3/2}$ have been calculated as 0.63 and 0.593, respectively.

Appendix C, Theoretical Determination of the Constant c

Substituting equation (11) into (6), we can find $w_l(y)$ as an explicit function of y:

$$w_l(y) = c\, w_* \left[1 - \exp(-y/D)\right]^{1/2} \exp(-y/D)\,, \tag{C1}$$

where w_* is the Deardorff velocity scale (equation 2). $w_l(y)$ is a nonmonotonic function, which approaches to zero at $y = 0$ and $y \to \infty$. Its maximum is

$$max(w_l) = c\, \frac{2}{3\sqrt{3}}\, w_* \approx 0.38\, c\;\, w_*. \tag{C2}$$

At the same time, we can also calculate the maximum of the characteristic vertical velocity for convection in homogeneous conditions as $max(\sqrt{\overline{w'^2}})$. Using the convective part in equation (B3), we find

$$max\sqrt{(\overline{w'^2})} = (1.2)^{1/3}\,(4/9)^{1/3}\,(3/5)^{1/2}\, w_* \approx 0.63\, w_*\,. \tag{C3}$$

Assuming that in the core of the plume convection is fully developed and that it is simlar to homogeneous conditions, we can assume that $max(w_l) = max\sqrt{(\overline{w'^2})}$. Hence, we obtain the estimation $c \approx 1.6$. We expect that this simple estimation, which neglects e.g., the mechanical part of the w-variance, is reasonable with 30 % accuracy.

Acknowledgments. We thank the associated editor and one of the referees for helpful comments and suggestions. This study was supported by the EU project DAMOCLES, which is financed in the 6th Framework Programme for Research and Development (grant 18509) and by DFG (grant no. LU 818/1-1). The LES runs were performed

on an IBM pSeries 690 supercomputer of the Norddeutscher Verbund für Hoch- und Höchstleistungsrechnern (HLRN).

References

Alam, A., and J. A. Curry (1997), Determination of surface turbulent fluxes over leads in arctic sea ice, *J. Geophys. Res., 102*, 3331–3344.

Andreas, E. L., Paulson, C. A., Williams, R. M., Lindsay, R. W., and J.A. Businger (1979), The turbulent heat flux from arctic leads, *Boundary-Layer Meteorol., 17*, 57–91.

Andreas, E. L., and B. Murphy (1986), Bulk transfer coefficients for heat and momentum over leads and polynyas, *J. Phys. Oceanogr., 16*, 1875–1883.

Andreas, E. L., and B. A. Cash (1999), Convective heat transfer over wintertime leads and polynyas, *J. Geophys. Res., 104 (C11)*, 25,721–25,734.

Beare, R. J, Cortes, M. A. J., Cuxart, J., Esau, I., Golaz, C., Holtslag, A. A. M., Khairoutdinov, M., Kosovic, B., Lewellen, D., Lund, T., Lundquist, J., Mccabe, A., Macvean, M. K., Moene, A., Noh, Y., Poulos, G., Raasch, S. and P. Sullivan (2006), An Intercomparison of Large-Eddy Simulations of the Stable Boundary Layer, *Boundary-Layer Meteorol., 118*, 247–272.

Birnbaum, G., and C. Lüpkes (2002), A new parameterisation of surface drag in the marginal sea ice zone, *Tellus A, 54A(1)*, 107–123.

Blackadar, A. K. (1962), The vertical distribution of wind and turbulent exchange in a neutral atmosphere, *J. Geophys. Res., 67*,3095–3102.

Brown, A. R. (1996), Evaluation of parameterization schemes for the convective boundary layer using large-eddy simulation results,*Boundary-Layer Meteorol., 81*, 167–200.

Deardorff, J. W. (1970), Convective velocity and temperature scales for the unstable planetary boundary layer and for Rayleigh convection, *J. Atmos. Sci., 27*, 1211–1213.

Deardorff, J. W. (1980), Stratocumulus-capped mixed layers derived from a three-dimensional model, *Boundary-Layer Meteorol., 18*, 495–527.

Dierer, S., and K.H. Schlünzen (2005), Atmosphere-sea ice interactions during cyclone passage investigated by using model simulations and measurements, *Month. Wea. Rev., 133, No.12*, 3678–3692.

Dierer, S., and K.H. Schlünzen (2005a), Influence parameters for a polar mesocyclone development, *Meteorol. Zeitschrift, 14*, 781–792.

Dyer, A. J. (1974), A review of flux-profile relationship, *Boundary-Layer Meteorol., 7*, 363–372.

Ertel, H. (1942), Der vertikale Turbulenz-Wärmestrom in der Atmosphäre, *Meteor. Z., 59*, 250–253.

Esau, I.N. (2007), Amplification of turbulent exchange over wide arctic leads: Large-eddy simulation study, *J. Geophys. Res., 112*, D08109, doi:10.1029/2006JD007225.

Frech, M., and L. Mahrt (1995), A two-scale mixing formulation for the atmospheric boundary layer, *Boundary-Layer Meteorology, 73, no. 1-2*, 91–104.

Glendening, J.W., and S.D. Burk (1992), Turbulent transport from an arctic lead: A large eddy simulation, *Boundary-Layer Meteorol., 59*, 315–339.

Gryanik, V.M., Hartmann, J., Raasch, S., and M. Schröter (2005), A refinement of the Millionshchikov quasi-normality hypothesis for convective boundary layer turbulence, *J. Atmos. Sci., 62*, 2632–2638.

Hartmann, J., Albers, F., Argentini, S., Bochert, A., Bonafe, U., Cohrs, W., Conidi, A., Freese, D., Georgiadis, T., Ippoliti, A., Kaleschke, L., Lüpkes, C., Maixner, U., Mastrantonio, G., Ravegnani, F., Reuter, A., Trivellone, G., and A. Viola (1999), Arctic Radiation and Turbulence Interaction Study (ARTIST), *Reports on Polar Research, Alfred Wegener Institute for Polar and Marine Research, Bremerhaven, 305*, 81 pp.

Hebbinghaus H., Dierer S., and K. H. Schlünzen K.H. (2006), Sensitivity studies on vortex development over a polynya, *Theoretical and Applied Climatology*, DOI 10.1007/s00704-006-0233-9.

Herbert, F., and G. Kramm (1985), Trockene Deposition reaktionsträger Substanzen, beschrieben mit einem diagnostischen Modell der bodennahen Luftschicht, Published in: Becker, K.H. and J. Löbel (Edts.): *Atmosphärische Spurenstoffe und ihr physikalisch-chemisches Verhalten., Springer Verlag, Berlin*, 264 pp.

Holtslag, A .A. M., and C. H. Moeng (1991), Eddy Diffusivity and countergradient transport in the convective atmospheric boundary layer, *J. Atmos. Sci., 48*, 1690–1698.

Kramm, G. (1995), Zum Austausch von Ozon und reaktiven Stickstoffverbindungen zwischen Atmosphäre und Biosphäre, *Schriftenreihe Fraunhofer Institut für Atmosphärische Umweltforschung, Bd. 34*, ISBN 3-927548-75-8, 268 pp.

Letzel, M. O., and S. Raasch (2003), Large-eddy simulation of thermally induced oscillations in the convective boundary layer, *J. Atmos. Sci., 60*, 2328–2341.

Lüpkes, C., and K. H. Schlünzen (1996), Modelling the arctic convective boundary-layer with different turbulence parameterisations, *Boundary-Layer Meteorol., 79*, 107–130.

Lüpkes, C., Hartmann, J., Birnbaum, G., Cohrs, W., Yelland, M., Pascal, R., Spiess, T., and M. Buschmann (2004), Convection over arctic leads (COAL), Published in

Schauer, U. and G. Kattner (Edts.): *The expedition ARKTIS XIX/1 a,b and XIX/2 of the Research Vessel Polarstern in 2003, Reports on Polar Research, Alfred Wegener Institute for Polar and Marine Research, Bremerhaven, 481*, 47–62.

Lüpkes, C., Vihma, T., Birnbaum, G., and U. Wacker (2008), Influence of leads in sea ice on the temperature of the atmospheric boundary layer during polar night, *Geophys. Res. Lett., 35*, L03805, doi:10.1029/2007GL032461.

Mauritsen T., Svensson, G., and B. Grisogono (2005), Wave flow simulations over arctic leads, *Boundary-Layer Meteorology, 117*, 259–273.

Mellor, G.L., T. and Yamada (1974), A hierarchy of turbulence closure models for planetary boundary layers, *J. Atmos. Sci., 31*, 1791–1806.

Monin, A. S., and A. M. Yaglom (1971), Statistical Fluid Mechanics, Vol. 1, MIT Press, Cambridge, USA.

Noh, Y., Cheon, W.-G., Hong, S.-Y., and S. Raasch (2003), Improvement of the K-profile model for the planetary boundary layer based on large eddy simulation data, *Boundary-Layer Meteorol., 107*, 401–427.

Paulson, C. A., and J. D. Smith (1974), The AIDJEX lead experiment, *AIDJEX Bull., 23*, 1–8.

Persson, P. O. G., Ruffieux, D., and C. W. Fairall (1997), Recalculations of pack ice and lead surface energy budgets during the Arctic Leads Experiment (LEADEX) 1992, *J. Geophys. Res., 102*, 25,085–25,089.

Pinto, J. O., Alam, A., Maslanik, J. A. Curry, J. A., and R. S. Stone (2003), Surface characteristics and atmospheric footprint of springtime arctic leads at SHEBA, *J. Geophys. Res., 108,* 8051, doi: 10.1029/2000JC000473.

Raasch, S., and G. Harbusch (2001), An Analysis of secondary circulations and their effects caused by small-scale surface inhomogeneities using large-eddy simulation, *Boundary-Layer Meteorol., 101*, 31–59.

Raasch, S., and M. Schröter (2001), A large-eddy simulation model performing on massively parallel computers, *Meteorol. Z., 10*, 363–372.

Ruffieux, D., Persson, P. O. G., Fairall, C. W., and D. E. Wolfe (1995), Ice pack and lead surface energy budgets during LEADEX 1992, *J. Geophys. Res., 100*, 4593–4612.

Schlünzen, K. H. (1988), Das mesoskalige Transport- und Strömungsmodell 'METRAS - Grundlagen, Validierung, Anwendung, *Hamburger Geophysikalische Einzelschriften, A88*, 139 pp.

Schlünzen, K. H. (1990), Numerical Studies on the inland penetration of sea breeze fronts at a coastline with tidally flooded mudflats. *Beitr. Phys. Atmosph., 63*, 243–256.

Schröter, M., Bange, J., and S. Raasch (2000), Simulated airborne flux measurements in a LES generated convective boundary layer, *Boundary-Layer Meteorol., 95*, 437–456.

Teixeira J., and S. Cheinet (2004) A simple mixing length formulation for the Eddy-diffusivity parameterization of dry convection, *Boundary-Layer Meteorol., 110(3)*, 435–453.

Troen, I. B., and L. Mahrt (1986), A simple model of the atmospheric boundary layer; sensitivity to surface evaporation, *Boundary-Layer Meteorol., 37*, 129–148.

Turner, J. S. (1986), Turbulent entrainment: the development of the entrainment assumption, and its application to geophysical flows, *J. Fluid Mech., 173*, 431–471.

Van Dop, H., and G. Verver (2001), Countergradient transport revisited, *J. Atmos. Sci., 58*, 2240–2247.

Vihma, T., Hartmann, J., and C. Lüpkes (2003), A case study of an on-ice air flow over the arctic marginal sea ice zone, *Boundary-layer Meteorol., 107*, 189–217.

Vihma, T., Lüpkes, C., J. Hartmann, and H. Sarvijärvi (2005), Observations and modelling of cold-air advection over arctic sea ice in winter', *Boundary-layer Meteorol., 117(2)*, 275–300.

Wacker, U., Potty, K. V. J., Lüpkes, C., Hartmann, J., and M. Raschendorfer (2005), A case study on a polar cold air outbreak over Fram Strait using a mesoscale weather prediction model, *Boundary-layer meteorology, 117(2)*, 301–336.

Weinbrecht, S., and S. Raasch (2001), High-resolution simulations of the turbulent flow in the vicinity of an arctic lead, *J. Geophys. Res., 106 (C11)*, 27,035–27,046.

Zilitinkevich, S., V. Gryanik, V. Lykossov, and D. Mironov (1999), Third-order transport and nonlocal turbulence closures for convective boundary layers. *J. Atmos. Sci., 56*, 3463–3477.

Zulauf, M.A., and S.K. Krueger (2003), Two-dimensional numerical simulations of arctic leads: Plume penetration height, *J. Geophys. Res., 108(C2)*, 8050, doi:10.1029/200JC000495.

8. Tables and Figures

Table 1. Summary of modelled 'cold' cases (ABL temperature: 250 K). u and v are the lead-orthogonal and lead-parallel components of the geostrophic wind, F_s is the average surface heat flux over the lead, F_{100} and F_{200} are the maximum upward fluxes of sensible heat at 100 m and 200 m height, α_p is the plume inclination.

	case 1 (weak-wind)	case 2	case 3 (medium-wind)	case 4 (strong-wind)	case 5
u (m s^{-1})	3.0	4.0	5.0	7.0	10.0
v (m s^{-1})	-0.4	-1.0	-1.0	-2.0	-2.5
F_s (W m^{-2})	123	155	170	223	270
F_{100} (W m^{-2}) (LES)	98	103	110	100	80
F_{100} (W m^{-2}) (METRAS)	88	92	95	98	90
F_{200} (W m^{-2}) (LES)	38	43	41	40	23
F_{200} (W m^{-2}) (METRAS)	42	42	41	42	40
α_p (degrees) (LES)	11.7	11.3	8.5	7.4	4.6
α_p (degrees) (METRAS)	11.3	11.0	8.0	6.3	4.6

Table 2. Summary of modelled 'warm' cases (ABL temperature: 260 K)

	case 1 (weak- (wind)	case 2	case 3 (medium- wind)	case 4 (strong- wind)	case 5
u (ms^{-1})	3.0	4.0	5.0	7.0	10.0
v (ms^{-1})	-0.4	-1.0	-1.0	-2.0	-2.5
F_s (W m^{-2})	51	61	72	89	121
F_{100} (W m^{-2}) (LES)	36	35	32	25	17
F_{100} (W m^{-2}) (METRAS)	28	31	31	30	30
F_{200} (W m^{-2}) (LES)	15	14	12	8	2
F_{200} (W m^{-2}) (METRAS)	12	12	13	12	11
α_p (degrees) (LES)	12.1	6.6	5.7	3.9	2.3
α_p (degrees) (METRAS)	10.6	6.6	4.9	3.6	3.0

Figure 1. Leads northeast of Svalbard (Aqua Modis image of 16 April 2005). The domain size is about 150 times 190 km^2.

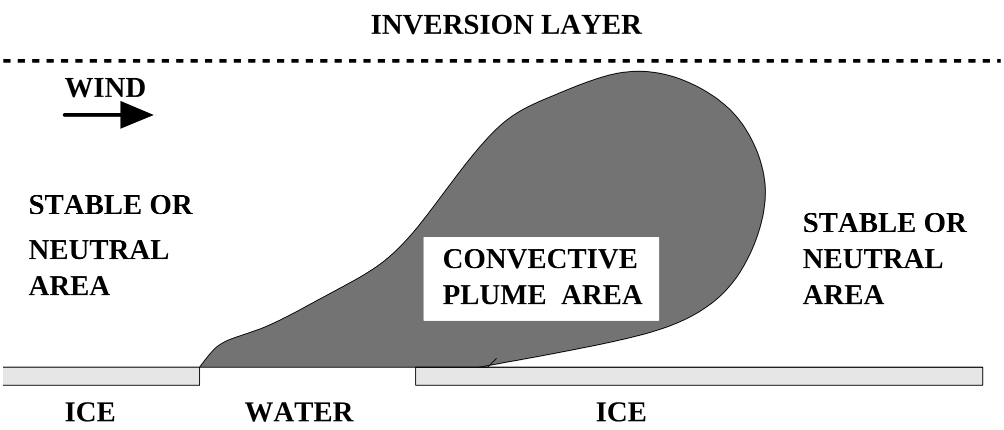

Figure 2. Schematic of the ABL over a polar lead during winter.

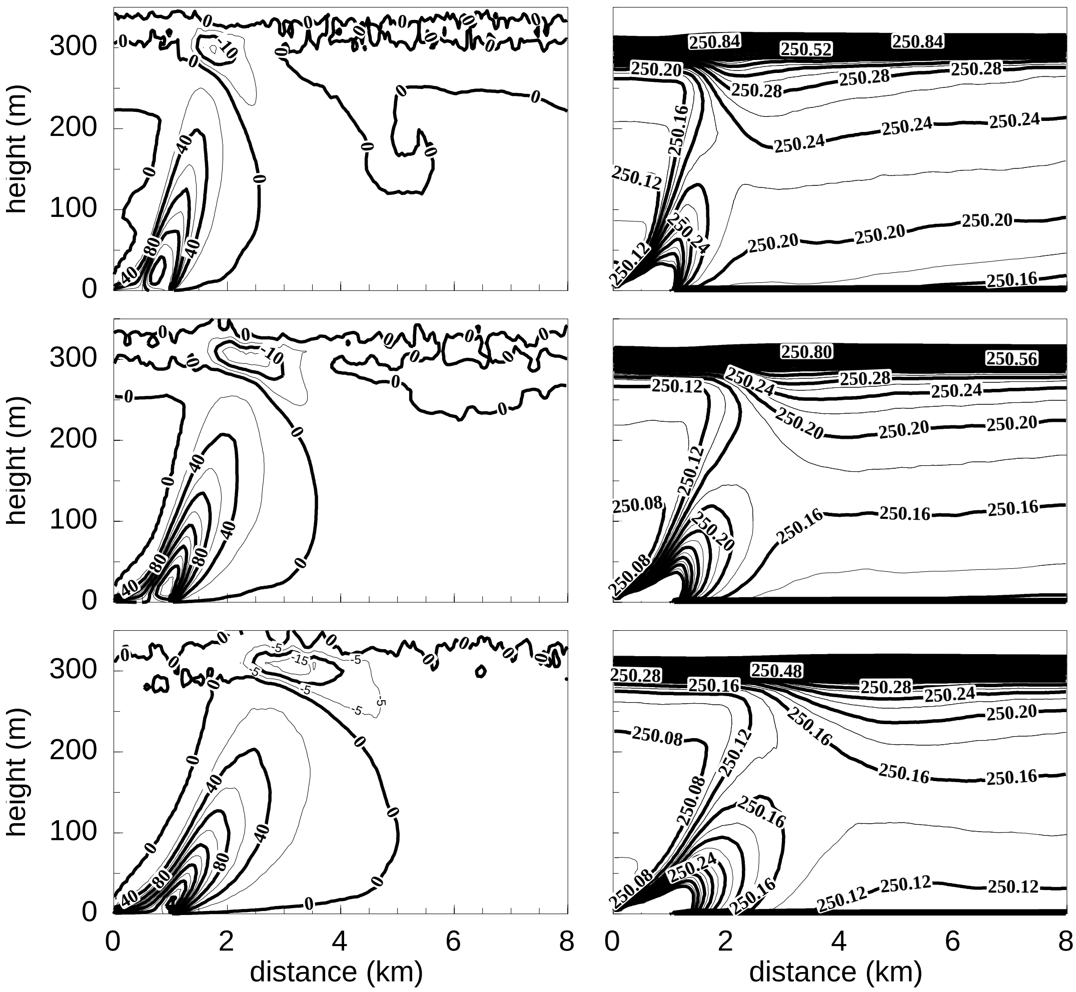

Figure 3. Sensible heat flux (left) in W m^{-2} and potential temperature in K (right) obtained from the LES model for the cold cases (top: weak-wind case, middle: medium-wind case, bottom: strong-wind case). The lead position is between 0 and 1 km distance. The surface wind is directed from left to right. The distance between contourlines is 5 W m^{-2} in case of downward fluxes.

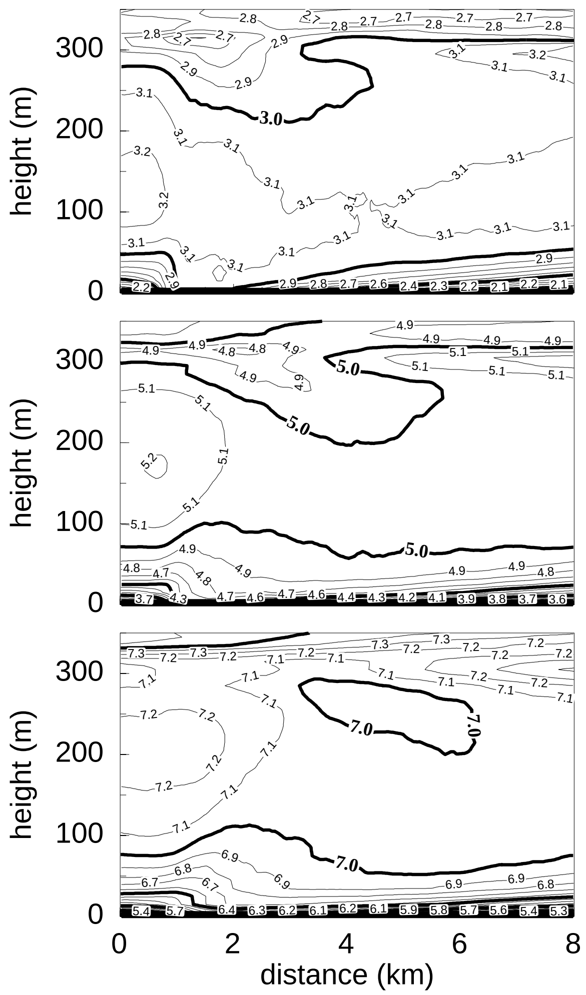

Figure 4. LES result as in Figure 3, but the absolute value of horizontal wind is shown in m s^{-1}.

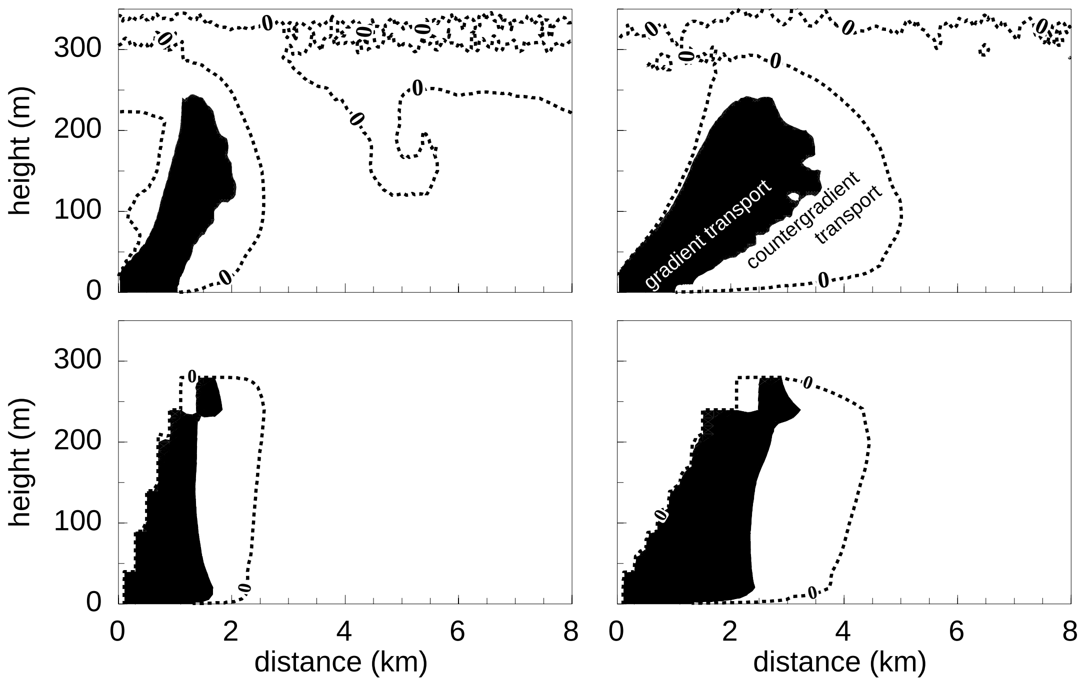

Figure 5. Regions with gradient and countergradient transport for the weak-wind (left) and strong-wind cold case (right) (top: LES, bottom: microscale model with the new closure of Section 5). The plume is defined as the area with upward heat flux (areas inside the dotted lines). In the dark areas the temperature decreases with height, everywhere else, it increases with height. Fluxes outside the plume are downward or zero.

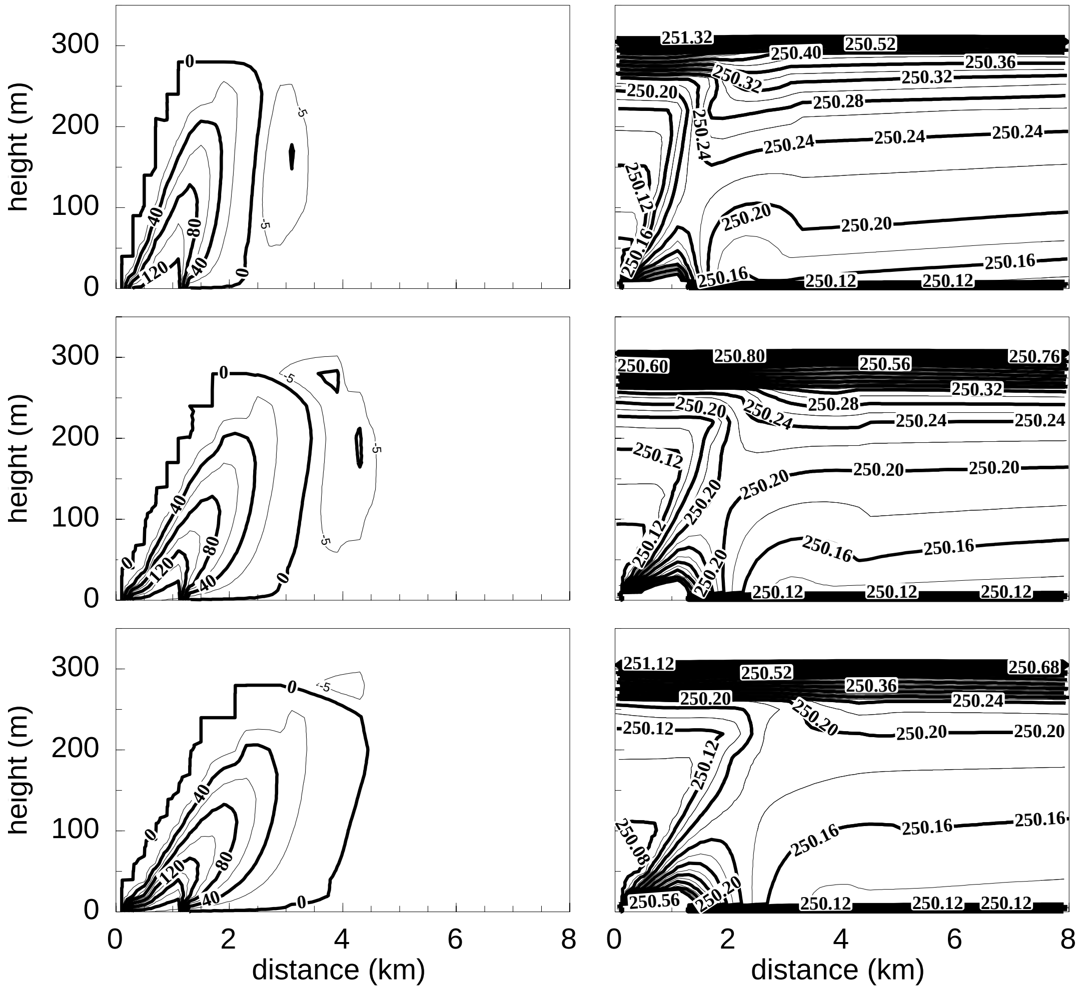

Figure 6. As Figure 3, but results were obtained with the microscale model using the new nonlocal closure derived in Section 5.

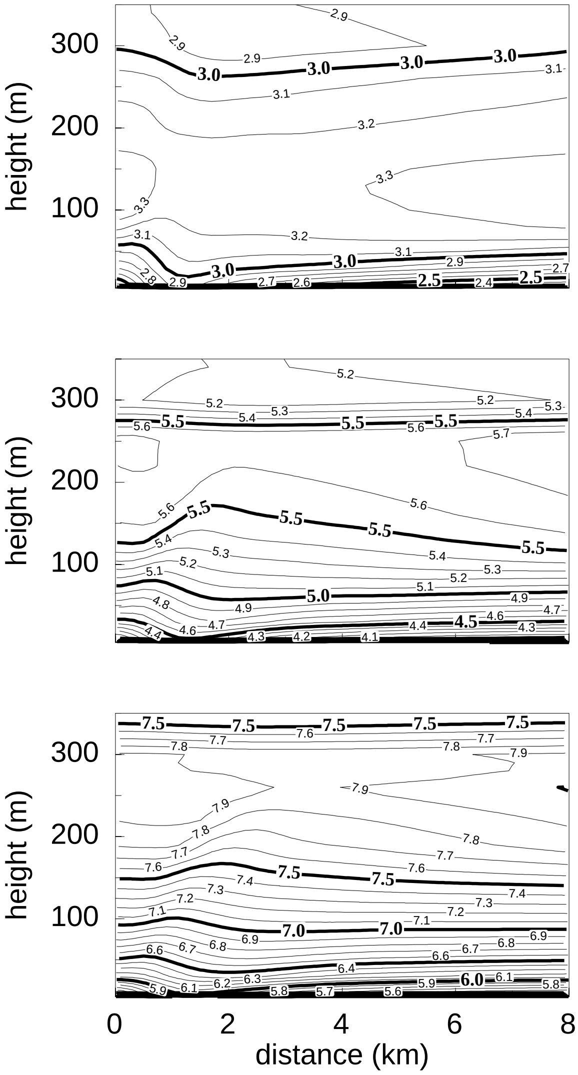

Figure 7. As Figure 6, but wind fields are shown (wind in m s^{-1}).

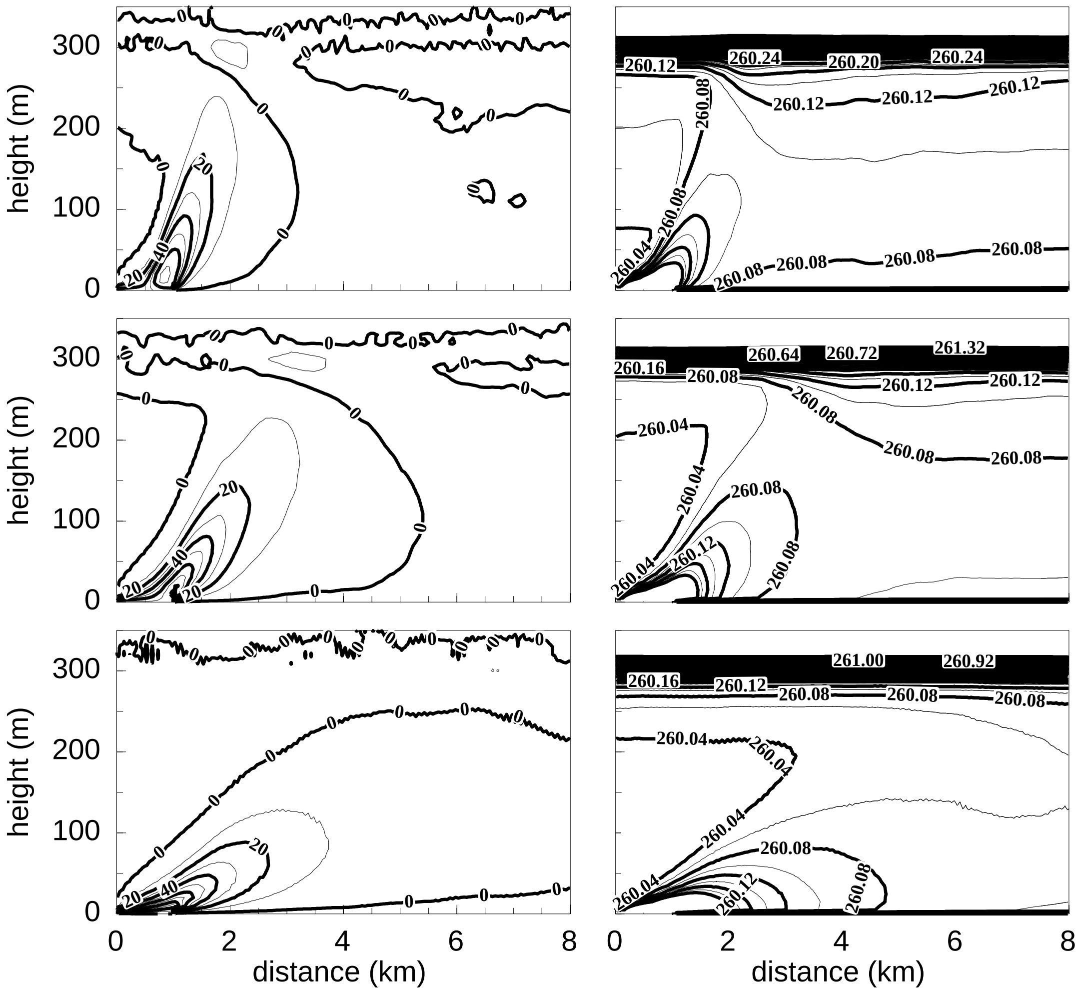

Figure 8. LES results as in Figure 3, but warm cases are shown.

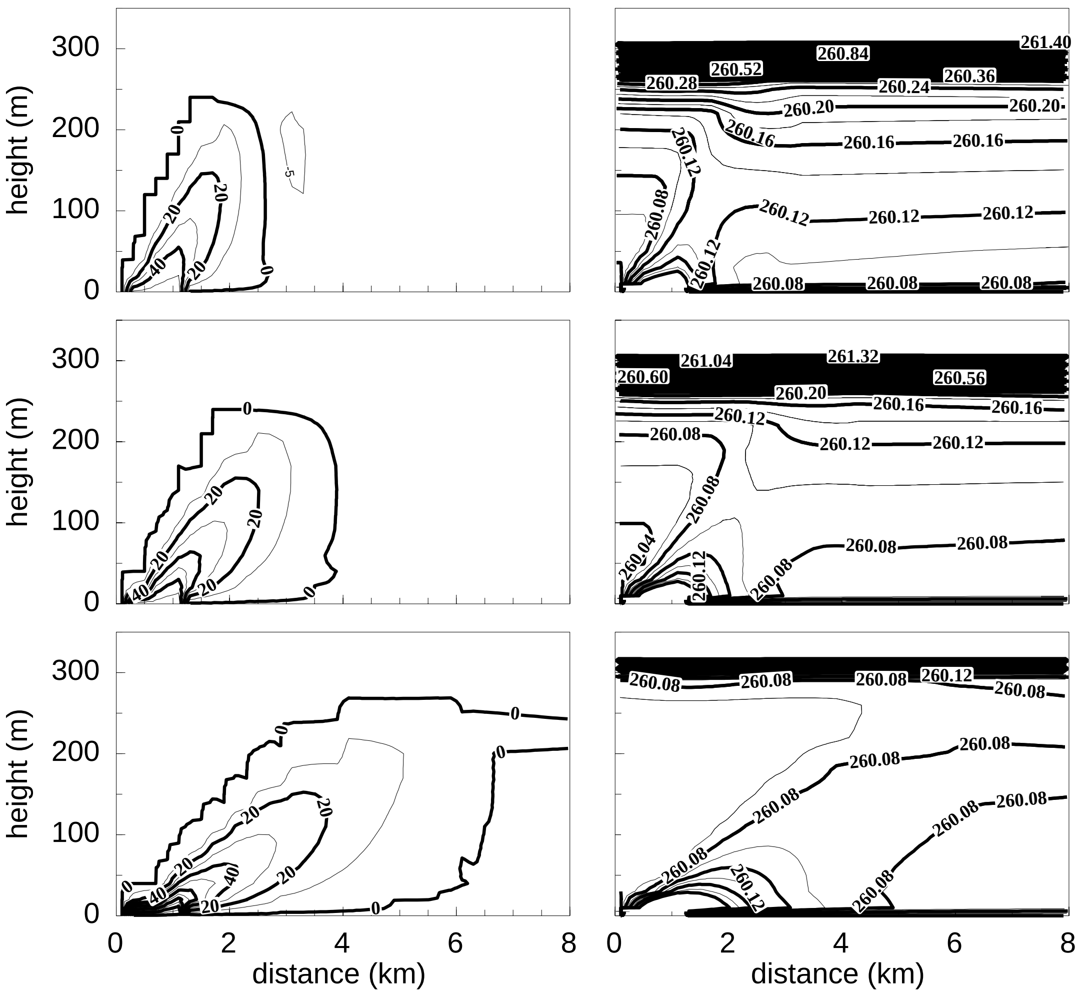

Figure 9. Results of the microscale model as in Figure 6, but warm cases are shown.

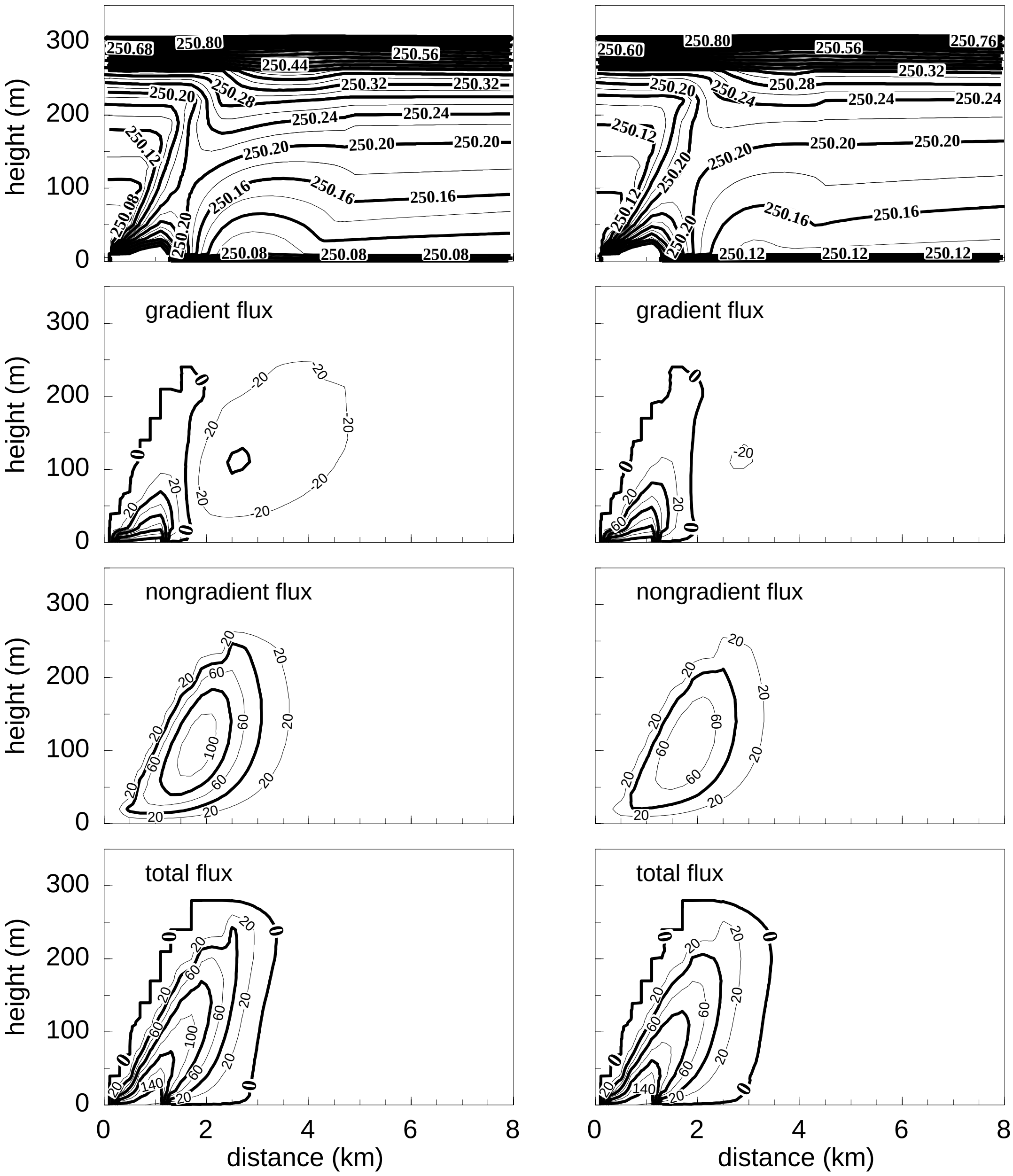

Figure 10. Results of the microscale model for the medium-wind cold case obtained with the new closure showing the sensitivity on the parameter b in the nonlocal term Γ given by equation (5) (left column: $b = 0.9$; right column: $b = 0.6$). Heat fluxes are given in W m^{-2}, pot. temperature in K.

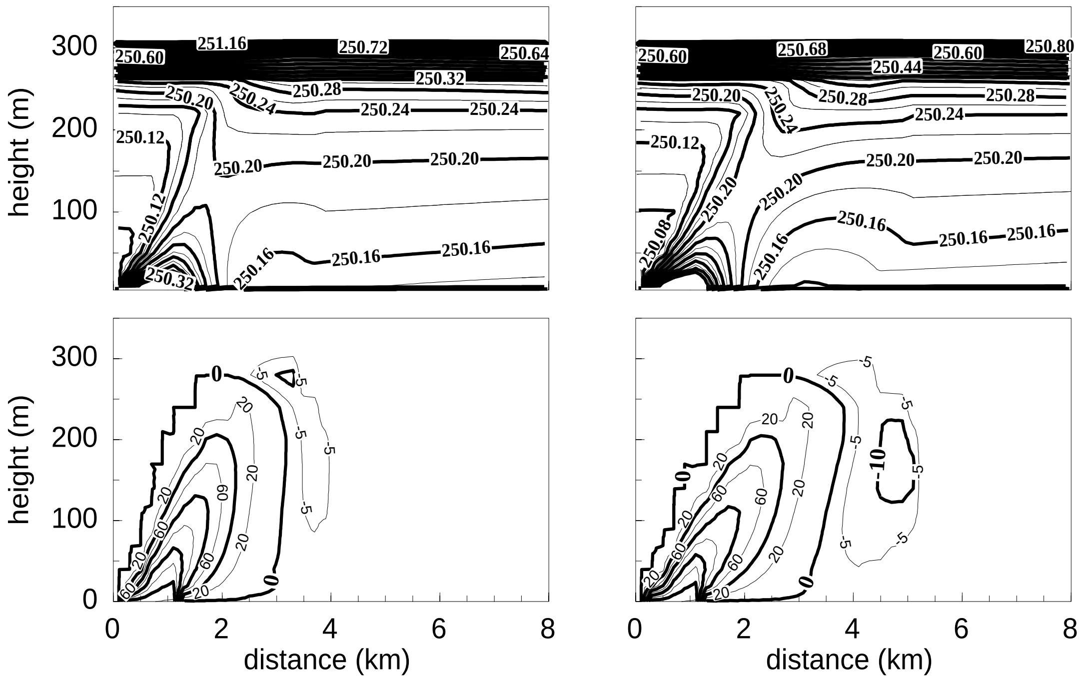

Figure 11. Results of the microscale model for the medium-wind cold case obtained with the new closure showing the sensitivity on the parameter a in equation (10) (left column: $a = 2.6$; right column: $a = 2.0$). Heat fluxes (bottom) are in W m^{-2}, pot. temperature (top) in K.

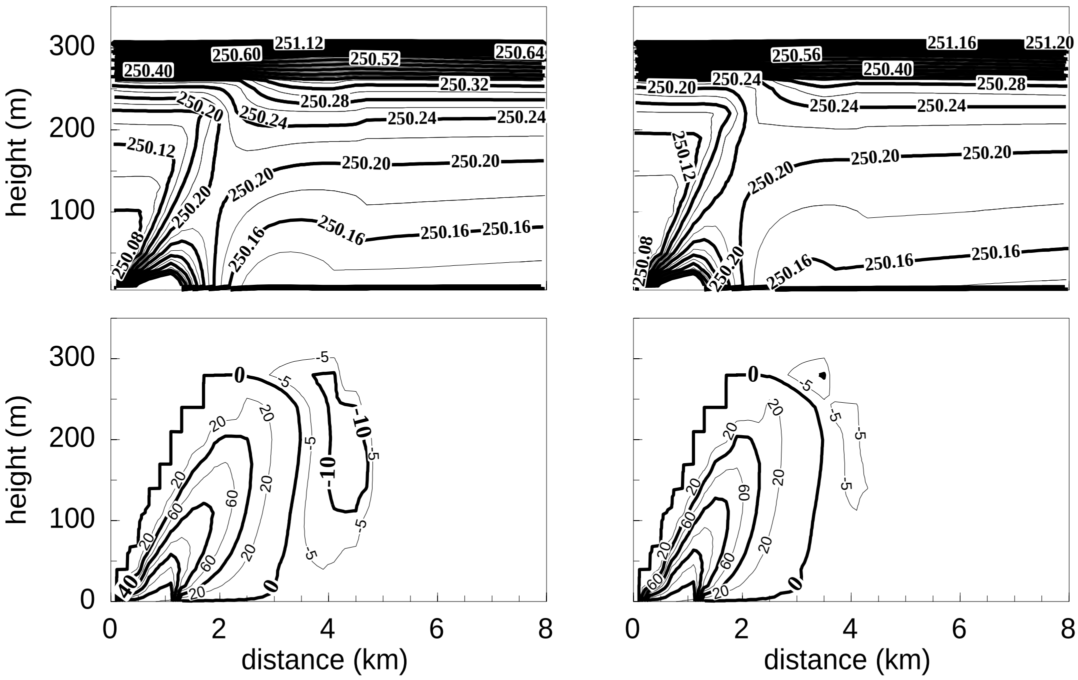

Figure 12. Results of the microscale model for the medium-wind cold case obtained with the new closure showing the sensitivity on the parameter c in equation (6) (left column: $c = 2.0$; right column: $c = 1.2$). Heat fluxes (bottom) are given in W m^{-2}, pot. temperature (top) in K.